JOURNAL OF GEOPHYSICAL RESEARCH, VOL. 114, C05015, doi:10.1029/2007JC004705, 2009

Observations of the Aleutian North Slope Current, Bering Sea, 1996–2001

P. J. Stabeno,[1] C. Ladd,[1] and R. K. Reed[1]

Received 19 December 2007; revised 14 January 2009; accepted 3 March 2009; published 14 May 2009.

[1] Cyclonic circulation dominates flow in the Bering Sea basin. The eastward flowing Aleutian North Slope Current (ANSC) flows along the north slope of the Aleutian Islands, turning northwestward in the southeast corner of the basin to form the Bering Slope Current (BSC). During the period 1997 to 2007, a pair of hydrographic lines was occupied 14 times in the southeastern portion of the basin. One transect was across the ANSC, and the second was across the BSC. In addition, a series of five yearlong moorings was deployed in a water depth of 1000 m in the ANSC, and a single yearlong mooring was deployed to the northeast in a water depth of 2200 m. At the primary mooring site, strong variability in temperature and salinity occurred at fortnightly and annual periods, while strong variability in the currents occurred at fortnightly and semiannual periods. The mean geostrophic flow relative to 1500 m, calculated from the 14 occupations of the hydrographic lines, was 3.1×10^6 m^3 s^{-1} in the ANSC and 3.3×10^6 m^3 s^{-1} in the BSC. A significant barotropic component, measured by the current meters, adds $\sim 3 \times 10^6$ m^3 s^{-1} to the transport.

Citation: Stabeno, P. J., C. Ladd, and R. K. Reed (2009), Observations of the Aleutian North Slope Current, Bering Sea, 1996–2001, *J. Geophys. Res.*, *114*, C05015, doi:10.1029/2007JC004705.

1. Introduction

[2] Our knowledge of the oceanography of the Bering Sea basin has advanced considerably over the last 25 years. A comprehensive early review [*Sayles et al.*, 1979] mapped water property distributions and geopotential topography (referred to 1400 and 2500 dbar) at various levels. Considerable information on the Bering Sea, as well as the subarctic Pacific in general, was also presented by *Favorite et al.* [1976]. More recently, *Johnson et al.* [2004] and *Wirts and Johnson* [2005] utilized Argo floats to explore water column properties and currents in the southeastern Bering Sea basin, and *Chen and Firing* [2006] described currents in the Bering Sea and subarctic North Pacific from Acoustic Doppler Current Profiler measurements from the summer of 1993.

[3] A cyclonic circulation dominates the flow in the upper water in the Bering Sea basin (Figure 1). Flowing eastward along the north slope of the Aleutian Islands is the Aleutian North Slope Current (ANSC), a narrow, high-speed current [*Reed and Stabeno*, 1999a]. Although an eastward flow along the northern side of the Aleutian Islands has been known for some time, its structure and transport were little known nor recognized as a continuous flow before the 1990s.

[4] The origin of the ANSC is the northward flow of the Alaskan Stream from the Pacific through various Aleutian Island passes [*Chen and Firing*, 2006; *Stabeno and Reed*, 1994]. This flow into the Bering Sea is an important source of nutrients, heat and salts for the ecosystem [*Mordy et al.*, 2005; *Stabeno et al.*, 2005]. The greatest inflow ($\sim 10 \times 10^6$ m^3 s^{-1}) [*Favorite*, 1974] occurs through Near Strait, with lesser though still significant transport through Amchitka Pass ($\sim 3 \times 10^6$ m^3 s^{-1}) [e.g., *Chen and Firing*, 2006; *Reed*, 1990] and Amukta Pass (4×10^6 m^3 s^{-1}) [*Stabeno et al.*, 2005]. With the exception of Amukta Pass, these transports are only approximations since few measurements have been made in these passes using moored current arrays [*Stabeno et al.*, 2005].

[5] While some eastward flow originating in the passes west of Amchitka Pass appears to continue past Bowers Ridge, it is estimated to be a small contribution to the ANSC [*Chen and Firing*, 2006; *Stabeno et al.*, 1999]. The majority of inflow of Alaskan Stream water through Near Strait (Figure 1) (maximum depth ~2000 m) is northward, turning cyclonically within the Bering Sea basin and eventually exiting southward through Kamchatka Strait [*Favorite et al.*, 1976; *Stabeno et al.*, 1999]. Other than Amukta Pass, most of the passes east of Amchitka Pass are shallow (<200 m) and the transport through each of them appears to be relatively small ($<0.4 \times 10^6$ m^3 s^{-1}) [*Stabeno et al.*, 2005]. That leaves only two likely sources for the majority of the ANSC: Amchitka Pass and Amukta Pass.

[6] The ANSC turns northwestward as it nears the eastern slope of the broad, eastern continental shelf, forming the Bering Slope Current (BSC), the eastern boundary current of the Bering Sea gyre. The BSC, through on-shelf fluxes, supplies critical nutrients to the shelf [*Stabeno et al.*, 2001; *Stabeno and Van Meurs*, 1999]. Since the BSC is a poleward extension of the ANSC, it is expected that the magnitude and variability of transport of the two currents would be similar. The character of the two systems, however, is very different. The BSC has weaker maximum speeds, tends to be rife with

[1]Pacific Marine Environmental Laboratory, NOAA, Seattle, Washington, USA.

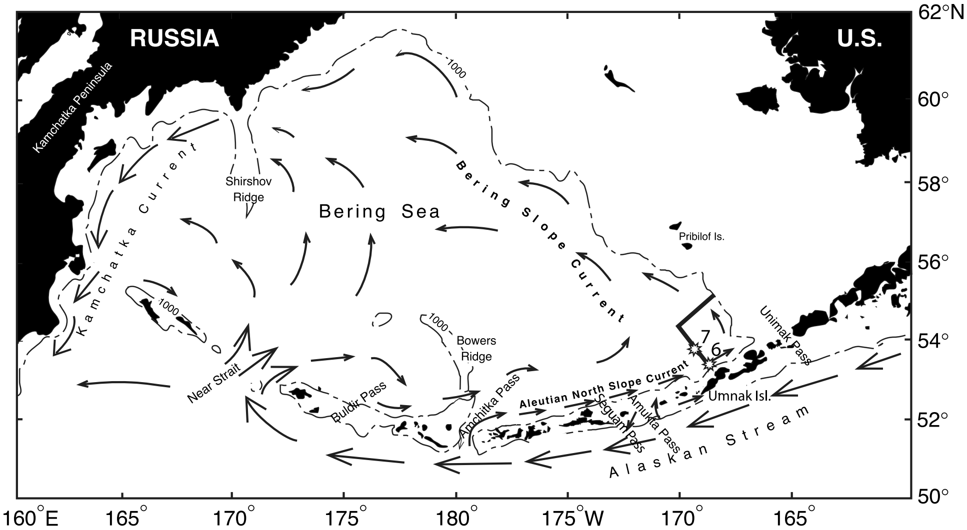

Figure 1. A schematic of the mean circulation in the Bering Sea basin is shown together with geographic locations. The positions of the two hydrographic lines are indicated by bold lines in the southeast corner of the basin. The locations of the two moorings are indicated by stars. Site 6 is the southern location, and Site 7 the northern location.

eddies and is often poorly defined [*Kinder et al.*, 1975]. In contrast, the ANSC is a narrow current with low-eddy kinetic/mean kinetic energy and higher maximum velocity [*Stabeno et al.*, 1999].

[7] The BSC flows northwestward along the slope. At approximately 58°N, a significant portion of the current separates from the slope and flows westward across the basin as a broad, weak flow [*Stabeno and Reed*, 1994]. The western boundary current of the Bering Sea gyre is the Kamchatka Current [*Favorite et al.*, 1976; *Panteleev et al.*, 2006; *Sayles et al.*, 1979; *Stabeno and Reed*, 1994], which flows southward through Kamchatka Strait to combine with remnants of the Alaskan Stream to form the Oyashio Current. Thus the Bering Sea gyre may be more aptly described as an extension of the Subarctic Gyre.

[8] This study, which focuses on the ANSC and the BSC, was made possible by an observational program conducted primarily during 1996–2002. An integration of hydrographic data collected on a series of cruises in the southeastern Bering Sea and data from moorings, which were deployed in the ANSC, is presented. On each of 14 cruises, CTD (conductivity, temperature, depth) casts were made to 1500 dbar (or near bottom in lesser depths) along two sections. One section crossed the ANSC while the other crossed the BSC. Each section, consisting of six or seven casts, was normal to the coastline or the 200-m isobath (Figure 1). Thus, a time series of water properties and geostrophic flow across the sections could be derived. In addition, direct measurement of currents, temperature and salinity (1996–2001) were made at Site 6 near one of the hydrographic stations in the ANSC, while 1 year of data was collected at a second mooring site, Site 7, farther north in the basin (Figure 1).

2. Methods

2.1. Geostrophic Flow

[9] Conductivity-temperature-depth (CTD) data were obtained on 14 cruises (Table 1) using a Seabird SBE9plus system with dual temperature and salinity sensors. Data were recorded during the downcast, with descent rate of 30 m min^{-1} to 200 m, then 45 m min^{-1}. Data from these cruises were used to derive the component of geostrophic flow normal to the section referred to 1500 dbar, or maximum common sample depth for the pair of stations closest to the shelf break (all >200 m). We do not imply that 1500 dbar is a level of no motion. In fact, mooring measurements show a significant barotropic component of flow. Only stations with separations greater than ~10 km were used to calculate transport and geostrophic flow. Because of the sharpness of bathymetry (especially along the Aleutian Islands) the depth of the inner (shallowest) station varied significantly. In addition, maximum geostrophic velocities often occurred between the last two stations, adjacent to the Aleutian Islands, implying that some of the transport is not completely captured by the sampling. However, the bathymetry shoals dramatically in a very short distance, so this unknown contribution to the ANSC transport is likely to be small.

2.2. Moorings

[10] Beginning in May 1996, a series of five yearlong moorings (Site 6) were deployed at a nominal depth of 1000 m in the ANSC. The bathymetry of this portion of the slope is characterized by sharp precipices. After a survey of the area, a narrow shelf at ~1000 m depth was selected for the mooring location. Only on the third deployment did we fail to hit the ledge, resulting in the mooring being deployed ~70 m deeper. Each mooring was a taut-wire with four current meters (nominal depths of 150, 300, 600, and 950 m). In addition to speed and direction, the current meter usually measured temperature, salinity and pressure. Temperature was also measured at nominal depths of 210, 240, 270, 330, 360, 390, 420, 450, and 500 m, and salinity at 240 m. The purpose of the relatively dense array of temperature sensors between 200 m and 450 m was to measure the subsurface temperature maximum that often occurs in the southeastern Bering Sea basin. All instruments sampled at hourly intervals.

Table 1. Summary of Geostrophic Flow Results

Dates	Northeastward Flow (ANSC) Transport (10^6 m^3 s^{-1})	Northeastward Flow (ANSC) Max Velocity (cm s^{-1})	Northwestward Flow (BSC) Transport (10^6 m^3 s^{-1})	Northwestward Flow (BSC) Max Velocity (cm s^{-1})
22–24 Feb 1997	3.2	25	3.6	24
11–13 Apr 1997[a]	5.3	23	5.8	39
15–17 Jun 1997	5.4	41	4.4	20
1–2 Jul 1997	8.8	84	6.8	39
23–25 Apr 1998	−1.3[b]	−23[b]	−2.2[b]	−21[b]
10–12 Feb 1999	3.5	19	3.8	13
13–14 May 1999	1.9	16	2.1	14
22–23 May 1999	1.7	38	4.4	19
25–26 Sep 1999[a]	4.4	17	4.4	14
20–22 Feb 2000[a]	6.6	29	5.2	25
27–29 Apr 2000	2.5	46	3.4	13
28–30 Aug 2000	2.8	27	4.6	17
10–11 May 2002	−3.7[b]	24	−1.8[b]	27
23–24 Apr 2007	2.8	34	1.0	17
Means	3.1 ± 3.1 (0.8 SE)		3.3 ± 2.6 (0.7 SE)	

[a]Sections shown in Figures 3 and 4.
[b]Note: negative numbers denote flow in the opposite direction from the long-term mean flow.

The current meter data were low-pass filtered with a 35-h, cosine-squared, tapered Lanczos filter to remove tidal and higher-frequency variability, and resampled at 6-h intervals.

[11] In 1996, a second mooring (Site 7) was deployed north of the primary mooring in ~2000 m water depth. It was similarly instrumented with four current meters (150, 300, 600, and 1800 m), one temperature/salinity recorder (240 m), and seven temperature recorders (210, 270, 330, 360, 390, 420, and 450 m). Data were collected at this site for only 1 year.

[12] A relatively high failure rate of the current meters at the southern mooring site was due to several causes. First, the anchors were deployed last and the top instruments were dragged through the water at relatively high speed, resulting in the loss of rotors. Second, the high (>100 cm s^{-1}) velocities in the ANSC at 150 m caused early failure of the rotors on the fifth deployment. Mechanical failures in the other years also limited data return.

2.3. Altimetry

[13] Gridded sea surface height anomalies (SSHA) with respect to a 7 year mean were downloaded from Aviso. The optimal interpolation methodology used by Aviso to merge data from multiple altimeters is described by *Le Traon et al.* [1998]. The mapped altimetry data set includes one map every 7 days with a 1/3° spatial resolution on a Mercator grid [Ducet et al. 2000; *Le Traon and Dibarboure*, 1999]. Merging data from multiple satellites with differing spatial and temporal resolution helps resolve the mesoscale, allowing for a better description of eddy activity [*Ducet et al.*, 2000; *Le Traon and Dibarboure*, 2004]. Global models used to detide the altimeter data do a good job in the deep ocean. However, the small errors in the estimates of deep ocean tides are amplified in shallow regions [*Cherniawsky et al.*, 2001]. Thus, we show SSHA only in regions with depths >200 m. Note that SSHA do not include the mean dynamic topography. Thus, it is impossible to distinguish eddies from meanders of the mean current in SSHA data. Hereafter, we use the word "eddy" to imply any roughly circular anomaly to the mean flow.

2.4. Wavelet Analysis

[14] Wavelet analysis was used to examine the dominant frequencies of the low-pass filtered salinity data at ~240 m. In contrast to Fourier analysis, wavelet analysis retains localized temporal information, a substantial advantage for analyzing nonstationary geophysical signals. The wavelet function used here was the Morlet wavelet with nondimensional frequency six, consisting of a sinusoid modulated by a Gaussian. We present the wavelet power spectra normalized by the variance of each time series. Because geophysical time series typically have red spectra (decreasing power over increasing frequency), we calculate 95% significance levels by comparing each wavelet power spectrum to a red noise background spectrum, modeled as univariate lag-1 autoregressive (AR-1) processes generated with variance equal to that of each time series [*Torrence and Compo*, 1998].

3. Satellite-Tracked Drifters

[15] Beginning in 1984, satellite tracked drifters (drogued at ~40 m) have been deployed in the North Pacific by investigators at our laboratory. At these northern latitudes, an average of ~15 position fixes per day are obtained from Argos. Over 400 drifters have been deployed in the Gulf of Alaska and the Bering Sea and their trajectories can provide insight into the flow pathways in this region [e.g., *Stabeno and Reed*, 1994].

[16] Trajectories of satellite-tracked drifters provided some of the first evidence of the high-speed current which flows along the north slope of the Aleutian Arc. Drifters deployed in the Gulf of Alaska were often advected southwestward in the Alaskan Stream, the western boundary current of the eastern subarctic gyre. Some of these drifters entered the Bering Sea through the Aleutian Passes and turned eastward into the ANSC (Figure 2). Eastward flow is evident in the trajectories north of the Aleutian Islands. The ANSC west of Amukta Pass (~172°W) is weaker and more convoluted (e.g., Figures 2a and 2b) than east of that pass. West of 172°W, net velocities were often < 20 cm s^{-1} toward the northeast while east of 172°W, they often exceeded 40 cm s^{-1} toward the northeast. Most drifters continued northeastward until intersecting the continental slope, where they either turned northwestward as part of the BSC (e.g., blue in Figure 2b) or were advected onto the shelf via Bering Canyon (e.g., red in Figure 2b).

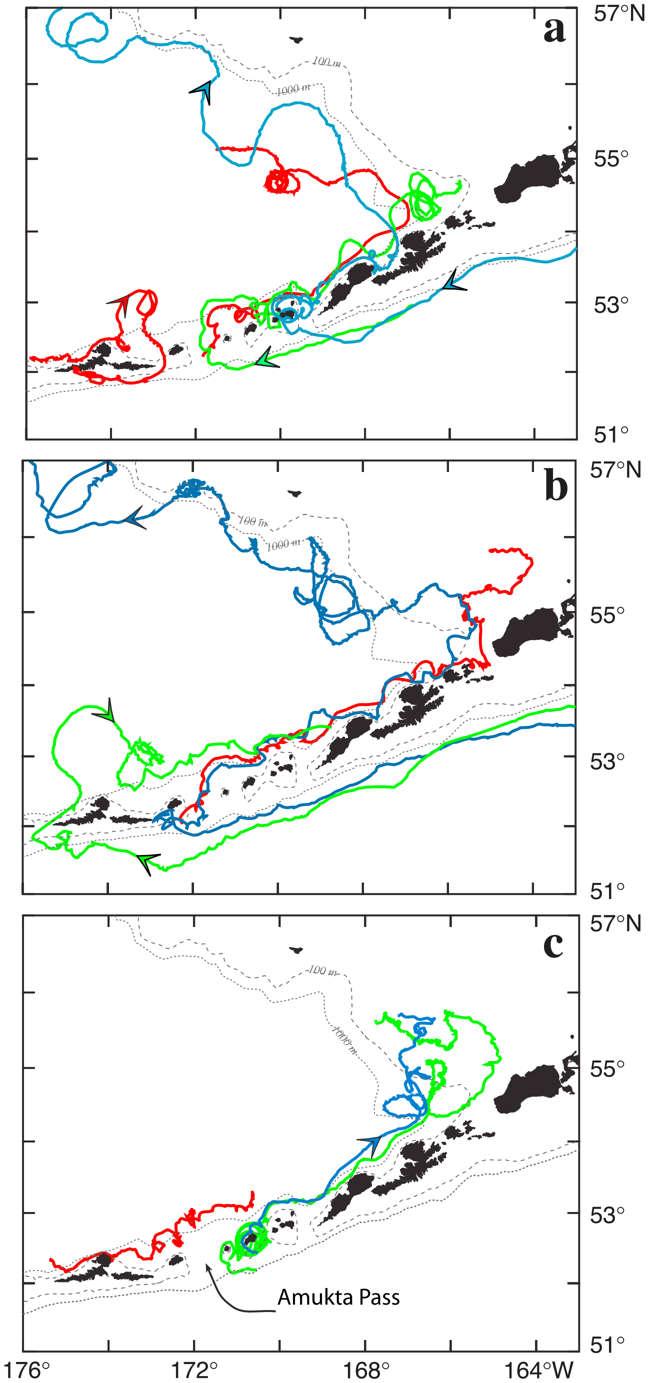

Figure 2. (a, b, c) Trajectories of a representative set of the over 300 satellite-tracked drifters deployed in the Gulf of Alaska and Aleutian Islands. The trajectories were chosen to show typical patterns, and Figures 2a, 2b, and 2c are purely for legibility. The depth of the drogues on these drifters was ~40 m. The flow is southwestward along the south side of the Aleutian Arc and northeastward along the north side.

[17] The differences in characteristics of flow in the ANSC and BSC are evident in these drifter trajectories. The ANSC, especially east of 172°W, is narrower and flow tends to follow bathymetry, while the BSC is broader and filled with eddies and meanders. Data collected on two hydrographic lines, one across the BSC and the second across the ANSC (Figure 1), further show the differing characteristics between the ANSC and BSC and are discussed next.

4. Geostrophic Flow Patterns, Speeds, and Transports

[18] Our focus is a comparison between the ANSC and the BSC (the southern section and the northern section, respectively, in Figure 1) in the southeast corner of the Bering Sea basin. Fourteen surveys across these two currents reveal high temporal variability in the system (Table 1). Large (radius >100 km) eddies in this region can be observed in altimetry data (Figure 3) and drifter trajectories (Figure 2) and are the cause of much of the variability. The eddies are typically formed south of the Pribilof Islands by meanders in the BSC and move slowly southwestward to influence the ANSC. Three surveys along with sea surface height anomalies (Figure 3) illustrate typical flow patterns and the influence of eddies on the flow.

[19] Maximum geostrophic velocities varied from 23 cm s^{-1} westward to 84 cm s^{-1} eastward in the ANSC and from 21 cm s^{-1} southeastward to 39 cm s^{-1} northwestward in the BSC. The geostrophic transports varied from 3.7×10^6 m^3 s^{-1} westward to 8.8×10^6 m^3 s^{-1} eastward in the ANSC and from 2.2×10^6 m^3 s^{-1} southeastward to 6.8 $m^3 \times 10^6$ s^{-1} northwestward in the BSC (Table 1). While the transports were not very sensitive to inclusion of the stations at the shallow part of the transects, maximum speed was. This was particularly true in the ANSC, where the depth of the shallowest station varied by >300 m. Also, because of the sharp bathymetry, the shallowest station was often ~10 km from its nearest neighbor, while elsewhere the separation was usually >30 km.

[20] In spite of the high spatial and temporal variability, mean transports (averaged over all surveys) on the northern and southern sections were not significantly different from each other (Table 1). Transports for both the ANSC and the BSC were $\sim 3 \times 10^6$ m^3 s^{-1} with standard deviations of $\sim 3 \times 10^6$ m^3 s^{-1} and standard errors ($S.E. = S/\sqrt{N}$, where S is the standard deviation and N is the number of samples) of 0.7–0.8 $\times 10^6$ m^3 s^{-1}. In addition, the correlation (r) between transports on the two sections was 0.89.

[21] The location of maximum speed differed between the two lines. On the southern line, 9 of the 14 sections had the highest speeds between the southernmost two stations (near Umnak Island). On the other five cruises, the flow was more unorganized. *Reed and Stabeno* [1999a] examined flow structure of the ANSC west of 175°W in 1990s and found a similar high-speed core along the Aleutian Islands with peak speeds often greater than 40 cm s^{-1} close inshore. Thus the highest velocities tended to occur on the steep bathymetric slope just offshore of Umnak Island. On the northern section, however, only six of the 14 sections had peak speeds between the northeasternmost two or three stations (near the 1000 m isobath). Thus flow on the northern section appears not to be "locked" to bathymetry, and peak speeds were relatively weak.

[22] The location of flow reversals also differed between the two sections. The flow offshore of the narrow, confined ANSC was weaker, unorganized and often influenced by eddies and/or meanders (Figure 3). On the southern section,

flow reversals tended to be well offshore (i.e., Figure 3b), and 4 of the 14 cruises had no significant (>0.010 dyn m) reversals (i.e., Figure 3c). On the northern section (BSC), 7 of the 14 sections had significant reversals (i.e., Figure 3a). On average, these reversals were on the eastern part of the section.

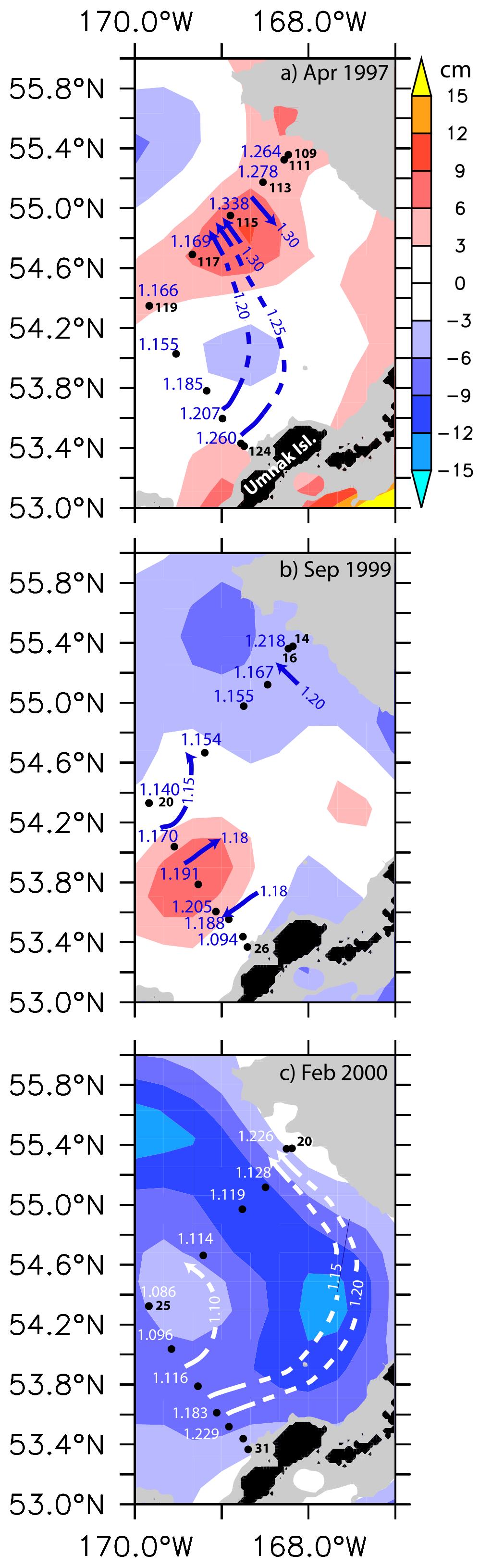

Figure 3. Geostrophic topography of the sea surface (in dyn m), referred to 1000 m during three different cruises (blue numbers and arrows). Sea surface height anomalies (in cm) from satellite altimetry (color) at the same time as the hydrographic surveys. Dashed blue lines indicate continuation of geostrophic contours (using the height anomalies to indicate probable paths) in region of no hydrographic data between the two transects. Location of hydrographic stations is indicated by black dots. Small black numbers indicate station number. The shelf (depth < 200 m) is indicated by gray area. Cruises were (a) 11–13 April 1997, (b) 25–26 September 1999, and (c) 20–22 February 2000.

[23] Although the timing of the 14 surveys is sparse temporally, there is some indication of interannual variability (Figure 4). The first four sections, February–July 1997, had the largest mean transports (5.7×10^6 m^3 s^{-1} for the ANSC and 5.2×10^6 m^3 s^{-1} for the BSC) (Table 1 and Figure 3a). The four sections during April 1998 to May 1999 had mean transports of only 1.5×10^6 (ANSC) and 2.0×10^6 m^3 s^{-1} (BSC). Finally for September 1999 to August 2000, mean transports increased to 4.1×10^6 (ANSC) and 4.4×10^6 m^3 s^{-1} (BSC). While the sampling does not permit a clear resolution of any annual cycle, the temporal variability does not appear to vary annually, but rather at longer periods. Certainly, the actual timescale of variability in transport cannot be determined with this data set.

[24] Transport through Amukta Pass near 172°W (maximum depth ~400 m) (Figure 1) has been studied often during the last decade. Although *Reed and Stabeno* [1997] presented computed geostrophic transports there (from nine hydrographic sections) and found a mean net northward transport of only 0.6×10^6 m^3 s^{-1} ($\pm 0.2 \times 10^6$ m^3 s^{-1}), transport measured from moorings at four sites (May 2001 to May 2003) revealed much higher transport averaging $\sim 4.0 \times 10^6$ m^3 s^{-1} [*Stabeno et al.*, 2005] with a strong barotropic component. The northward flow in Amukta Pass is predominantly on the eastern side, with a weaker southward flow occurring in the western part of the pass. This northward transport can account for a significant portion of the transport in the ANSC listed in Table 1.

[25] The other likely source of the ANSC is flow through Amchitka Pass (near 180°, depth ~1300 m (Figure 1)). Table 2 summarizes the volume transports computed from CTD data at seven sites located along 51.5°N in an east–west section across Amchitka Pass. Like Amukta Pass, there often appears to be northward flow on the east side and southward flow on the west side of the pass. The occupation of the Amchitka Pass section during May 1997 was close in time to the three sections in spring and early summer 1997 across the ANSC (Table 1). For these three occupations, the mean transport in the southern sections was 6.5×10^6 m^3 s^{-1}, and in the northern section was 5.7×10^6 m^3 s^{-1} (Table 1). This is in excellent agreement with the northward branch of flow (6.1×10^6 m^3 s^{-1}) on the eastern side of Amchitka Pass (Table 2).

[26] Approximately 1 year later, the flow in the ANSC and BSC had reversed to flow counter to the mean direction with transport of $\sim 1 \times 10^6$ m^3 s^{-1} (Table 1). The northward flow (5.5×10^6 m^3 s^{-1}) in Amchitka Pass at that time was on the western side of the pass. From limited data at 178°W, 175°W, and 172.5°W, the flow through Amchitka did not appear to

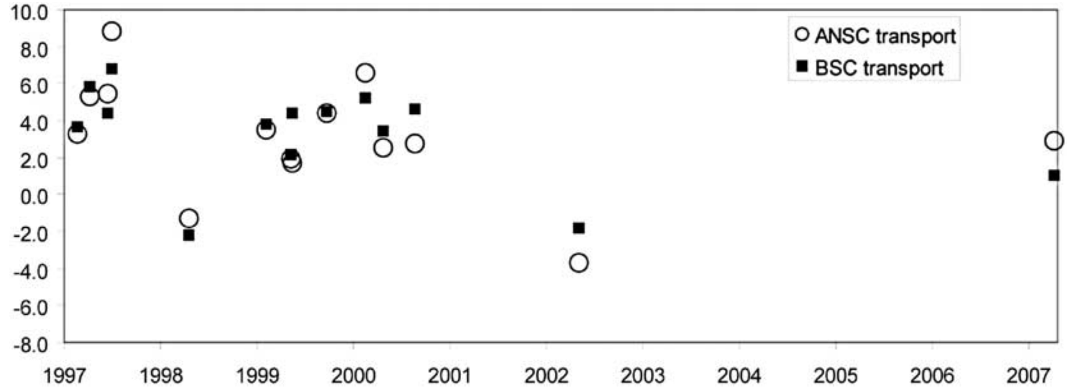

Figure 4. Geostrophic transport in the ANSC (circles) and the BSC (squares) from Table 1.

continue eastward north of the Aleutians. The most likely explanation is that southward flow (4.0×10^6 m^3 s^{-1}) on the eastern side of the pass was a retroflection of the northward flow on the western side of the pass. Thus the net flow through Amchitka Pass in June 1998 was 1.5×10^6 m^3 s^{-1} northward (Table 2), of which some portion may have turned eastward contributing to the ANSC. Thus a period of high transport (low transport) in the ANSC corresponded to a period of strong (weak) northward flow through Amchitka Pass. The other three occupations of Amchitka Pass show a range of variability similar to those observed in the ANSC.

[27] The most likely scenario is that the ANSC transport east of Amukta Pass has two main components. Some portion of the northward flow through Amchitka Pass turns eastward and flows along the north slope of the Aleutian Islands. This pattern is observed in drifter trajectories and hydrography. Some of this eastward flow exits the Bering Sea through the western portions of the passes, especially Amukta Pass. Inflow in the eastern side of Amukta Pass and the other smaller Aleutian Passes then combines with the eastward flowing ANSC increasing the transport. While some eastward flow originating in the passes west of Amchitka Pass may continue past Bowers Ridge, it is estimated to be a small contribution to the ANSC [*Chen and Firing*, 2006; *Stabeno et al.*, 1999].

5. Vertical Structure and Seasonality

[28] To investigate the vertical structure and seasonality of the water masses in the ANSC and BSC, hydrography from the same three surveys shown previously (Figure 3) is presented (Figure 5). Note that at the temperatures that occur below ~100 m in the Bering Sea, density is primarily determined by salinity. Thus contours of salinity in Figure 5 look much like those of density (not shown). In both the ANSC and the BSC, ~80% of the station pairs had maximum geostrophic velocity at the sea surface, while the others had peak velocities near 100 dbar.

5.1. Early Spring

[29] In the Bering Sea, April is at the end of winter, before the significant summer heating warms the surface waters. In April 1997 (Figure 5a), sea surface temperature was ~4°C, with a subsurface temperature maximum (>4°C) occurring at ~100–400 dbar. Fresher water (<32.8) was observed within ~20 km of the Aleutian Islands and extended over a broader area (~90 km) on the northern line. The sharp downward slope of isotherms and isohalines in the upper 500 m along Umnak Island are indicative of the well-developed eastward flow along the island. Calculations show a subsurface maximum speed of more than 20 cm s^{-1} (near 100 dbar) (Table 1). Elsewhere in the southern section, near-surface flow was weak. On the northern section, the maximum speed was at the surface. It was stronger (39 cm s^{-1}) than on the southern section, and offshore of the shelf break on the western edge of the lens of fresher surface water. Near the shelf break, southeastward flow occurred. The depression of the isotherms and isohalines at Station 115, and the fresher lens of surface water were related to the anticyclonic eddy evident in the map of sea surface height anomalies (Figure 3a).

5.2. Late Summer

[30] In late summer (September 1999) (Figure 5b), near surface temperatures were warmer by more than 4°C than those measured in April 1997. Surface temperatures were greater than 8.3°C except at the two stations nearest Umnak Island where surface temperatures were between 6.6°C and 7.0°C. The subsurface temperature maximum (>3.6°C at 200–300 dbar) was cooler than in April and the subsurface minimum (a remnant of the previous winter cooling) was evident as small areas of water cooler than 3.6°C between 100 and 150 dbar (in both the ANSC and the BSC). The subsurface temperature minimum provides evidence that this water has been in the Bering Sea since the previous winter.

[31] Salinity was little different from April except near the surface, where a layer of fresher water (<32.8) associated

Table 2. Geostrophic Transports Through Amchitka Pass

Date	Northward Flow (10^6 m^3 s^{-1})	Southward Flow (10^6 m^3 s^{-1})	Net Flow (10^6 m^3 s^{-1})
August 1991	1.6	4.4	2.8 south
September 1992	2.6	1.8	0.8 north
September 1993	4.1	1.3	2.8 north
May 1997	6.1	2.1[a]	4.0 north
June 1998	5.5[b]	4.0[b]	1.5 north
Mean	4.0	2.7	1.3 north
SD	±1.9	±1.4	±2.6

[a]The 2.1×10^6 m^3 s^{-1} southward flow did not seem to be a retroflection from the northward flow, but rather a separate flow along the eastern side of Bowers Ridge [*Reed and Stabeno*, 1999b].

[b]Typically, the northward flow is on the eastern side of the passes, while southward flow is on the western side. In June 1998, the northward flow was on the western side of Amchitka Pass, and the southward flow was on the eastern side.

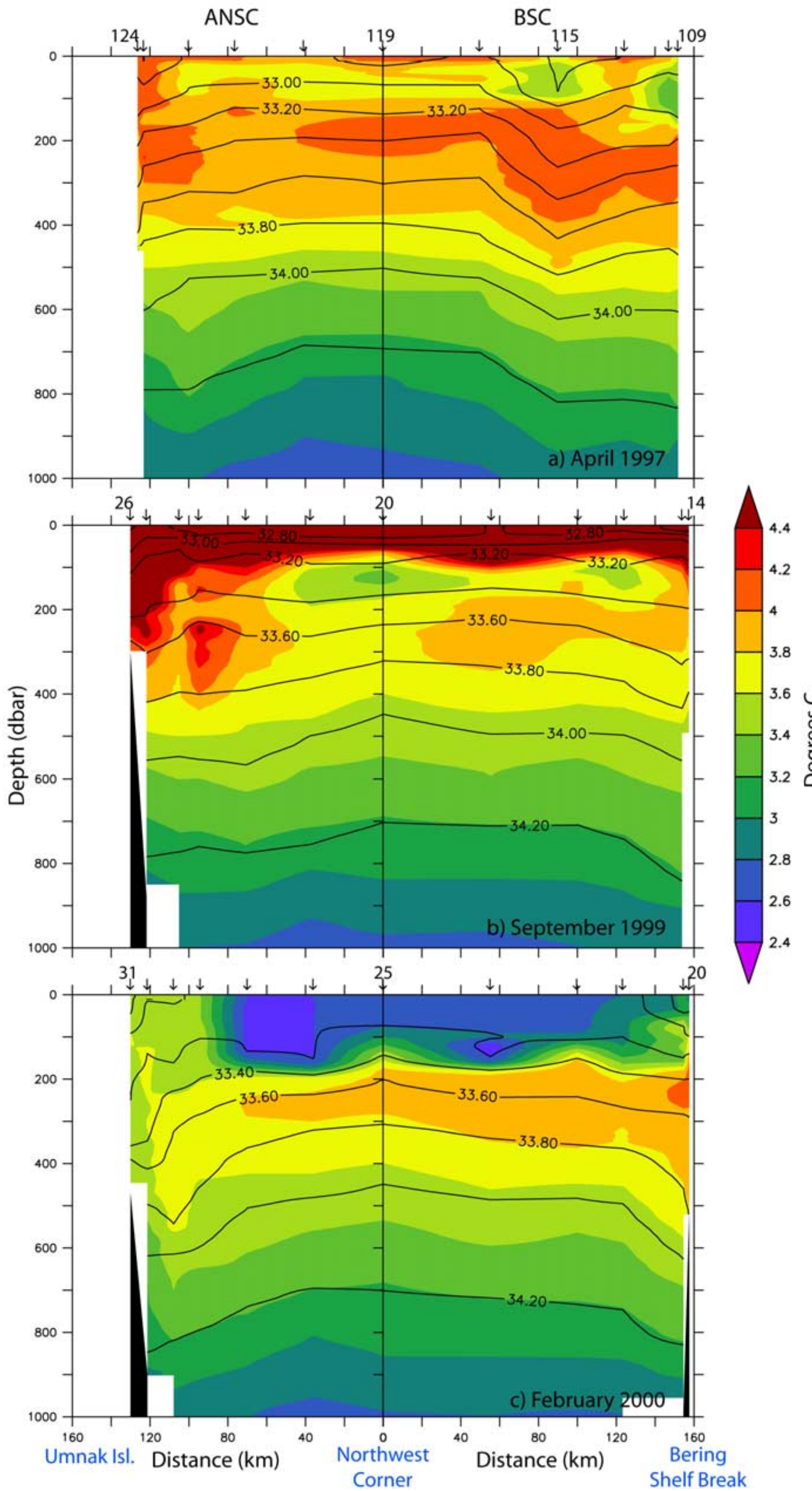

Figure 5. Potential temperature (in °C; color) and salinity (contours) on the two transects (ANSC and BSC) for the same three cruises shown in Figure 3. Cruises were (a) 11–13 April 1997, (b) 25–26 September 1999, and (c) 20–22 February 2000. Arrows indicate the station locations.

with the surface mixed layer was observed. The probable source of the fresher water was the Alaska Coastal Current which flows through the shallow passes east of 170°W [*Ladd et al.*, 2005; *Stabeno et al.*, 2005, 2002].

[32] The source of the deeper water (200–400 dbar) in the ANSC with temperatures >4°C was likely Amukta Pass. Amukta Pass is approximately 200 km away from the southern section. At a velocity of 20 cm s^{-1}, it would take ~10–15 days for water from Amukta to reach the section. The bulk of the water flowing through Amukta Pass deeper than 100 m is in the same temperature, salinity, and density range [e.g., *Ladd et al.*, 2005; *Reed and Stabeno*, 1994] as the subsurface temperature maximum.

5.3. Winter

[33] During winter (February 2000), sea surface temperatures were cooler (generally <3°C) (Figure 5c), approximately 1°C less than surface conditions in April and the mixed layer was deeper. Because of the deeper mixing, surface salinities (except next to the shelf break) were higher in the winter than in either April or September. The subsurface temperature maximum was also cooler than observed in spring and similar to that observed in September 1999.

6. Time Series of Temperature, Salinity, and Currents

[34] The hydrographic sections provide insight into the spatial patterns and extent of the ANSC/BSC system. Data from the two mooring sites provide a more detailed view of how the currents, temperature and salinity vary on a continuum of periods from hours to years. Both moorings were on the southern transect (Figure 1). The southern mooring site (Site 6) was in the region where maximum geostrophic flow typically occurred as previously discussed. The other mooring site (Site 7) was north of the high-speed core in a region of greater variability and relatively weak flow.

6.1. Temperature

[35] The series of moorings at the southern site provided data showing the temporal variability of the high-speed core of the ANSC over a period of almost 5 years (Figure 6). While in the Bering Sea density is primarily dependent on salinity below 100 m, temperature is a useful tracer. In addition, temperature measurements are more reliable than those of salinity.

[36] The annual evolution of subsurface temperatures is influenced by mixing in the Aleutian Passes upstream. The top instrument at Site 6 was nominally at 150 m, so we cannot see the evolution of the local surface mixed layer especially during the warm season, but an annual signal is evident throughout the water column during each year. Maximum temperatures occurred progressively later with depth. At ~150 m, maximum temperature occurred in October, while at ~500 m, warmest temperatures occurred in December or early January; at ~1000 m, maximum temperatures occurred in January (Figure 6). The likely cause of the annual signal at 500 m is a result of mixing in the passes. Large mixing coefficients (>10^{-2} m^2 s^{-1}) near the crest of the Aleutian Ridge (Amukta Pass) were evident in model runs [*Cummins et al.*, 2001]. As already mentioned, Amukta Pass (~250 km upstream of the mooring) and Amchitka Pass (~750 km upstream) likely supply most of the flow in the ANSC. The strong tidal currents in many of the passes tend to partially mix the water column vertically. For instance, in nearby Seguam Pass (Figure 1) (water depth ~150 m) temperature data was collected from a mooring during 2002 [*Stabeno et al.*, 2005]. The water column in Seguam Pass was largely well mixed May through early July, while during September, it was weakly stratified with a maximum temperature of ~6.5°C at 40 m and 5°C at 130 m. Presumably in October, surface cooling and enhanced winds combine with the tidal currents to mix the water column in Seguam Pass top to bottom. The timing (October) of the warmest temperatures at ~150 m is consistent with flow through Amukta Pass (~400 m deep) being partially mixed vertically in the pass and then advected eastward in the ANSC.

[37] Of more interest is the warming at 600–900 m that occurs from May to January of each year. One possible source of this deeper water is Amchitka Pass, which at >1200 m, is much deeper than Amukta Pass. Strong vertical mixing is not evident in hydrographic sections across Amchitka Pass [e.g., *Stabeno et al.*, 1999, Figure 6]. However, these sections were all sampled in warm seasons, not during winter. Another possible explanation for this warming signal is a vertical shift of the hydrographic structure. Winds during these months are predominantly westerly causing downwelling north of the Aleutian Islands. This could also explain the warmer waters at depth.

[38] Seasonal warming below 300 m is also evident at Site 7 (the northern mooring) in 1996 (Figure 7), although an annual signal below 500 m is not evident. The upper instrument was much deeper (~300 m) at this location than at the southern mooring, and the maximum temperature (~4.75°C) appears in early December, approximately one month later than the maximum temperature at Site 6.

[39] In addition to the annual signal, variability also occurs on shorter periods. A strong fortnightly tidal signal is evident in the spectra (not shown) of the bottom (+50 m) temperature records at Site 6 and is also evident in the transport through Amukta Pass [*Stabeno et al.*, 2005]. While it is difficult to pick out a fortnightly signal in the shallower records at the northern mooring site (Site 7), there is a well-defined fortnightly signal at the deepest temperature record (~2000 m).

[40] At the northern site (Figure 7), several sharp, episodic events were observed where the isotherms deepened and remained depressed for approximately a month (e.g., 3.5°C isotherm in March). These are likely the signature of the large anticyclonic eddies that are common in this region. Such eddies were often observed in the temperature/salinity data from a mooring deployed at 54.8°N, 168.6°W to the northeast of Site 7 [*Cokelet and Stabeno*, 1997]. The signature of

Figure 6. (a, b, c, d, e) Temperature (in °C; color) and daily current vectors (rotated 30°) measured at the series of moorings deployed at Site 6. Figures 6a, 6b, 6c, 6d, and 6e each represent one deployment. The currents have been low-pass filtered and rotated so that up represents currents to the northeast paralleling bathymetry. The position of the current time series indicates the approximate depth of instrument. Gaps in the records are due to failure of equipment.

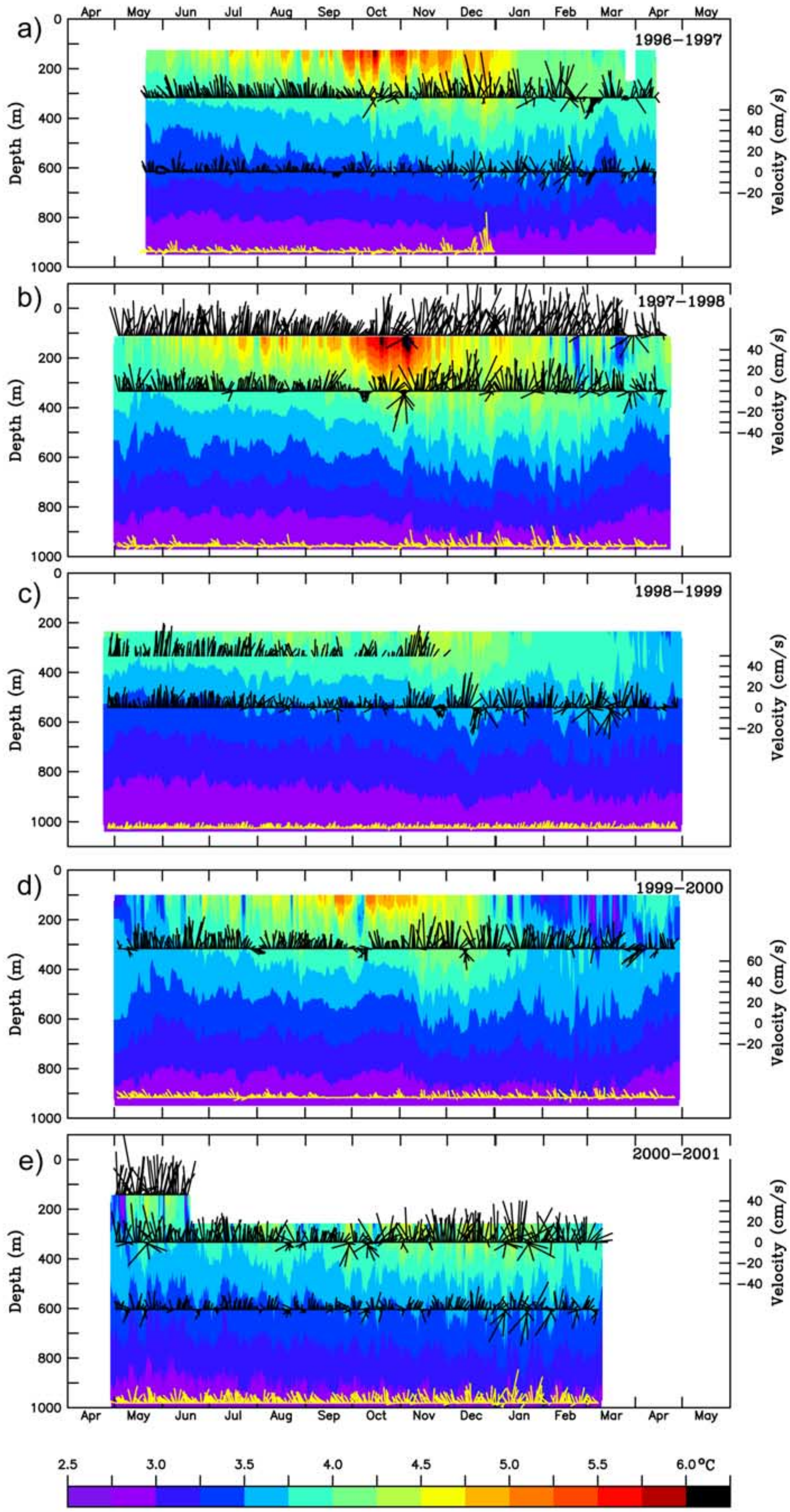
a)
1996–1997
b)
1997–1998
c)
1998–1999
d)
1999–2000
e)
2000–2001
Depth (m)
Velocity (cm/s)
Apr
May
Jun
Jul
Aug
Sep
Oct
Nov
Dec
Jan
Feb
Mar
2.5
3.0
3.5
4.0
4.5
5.0
5.5
6.0°C

Figure 6

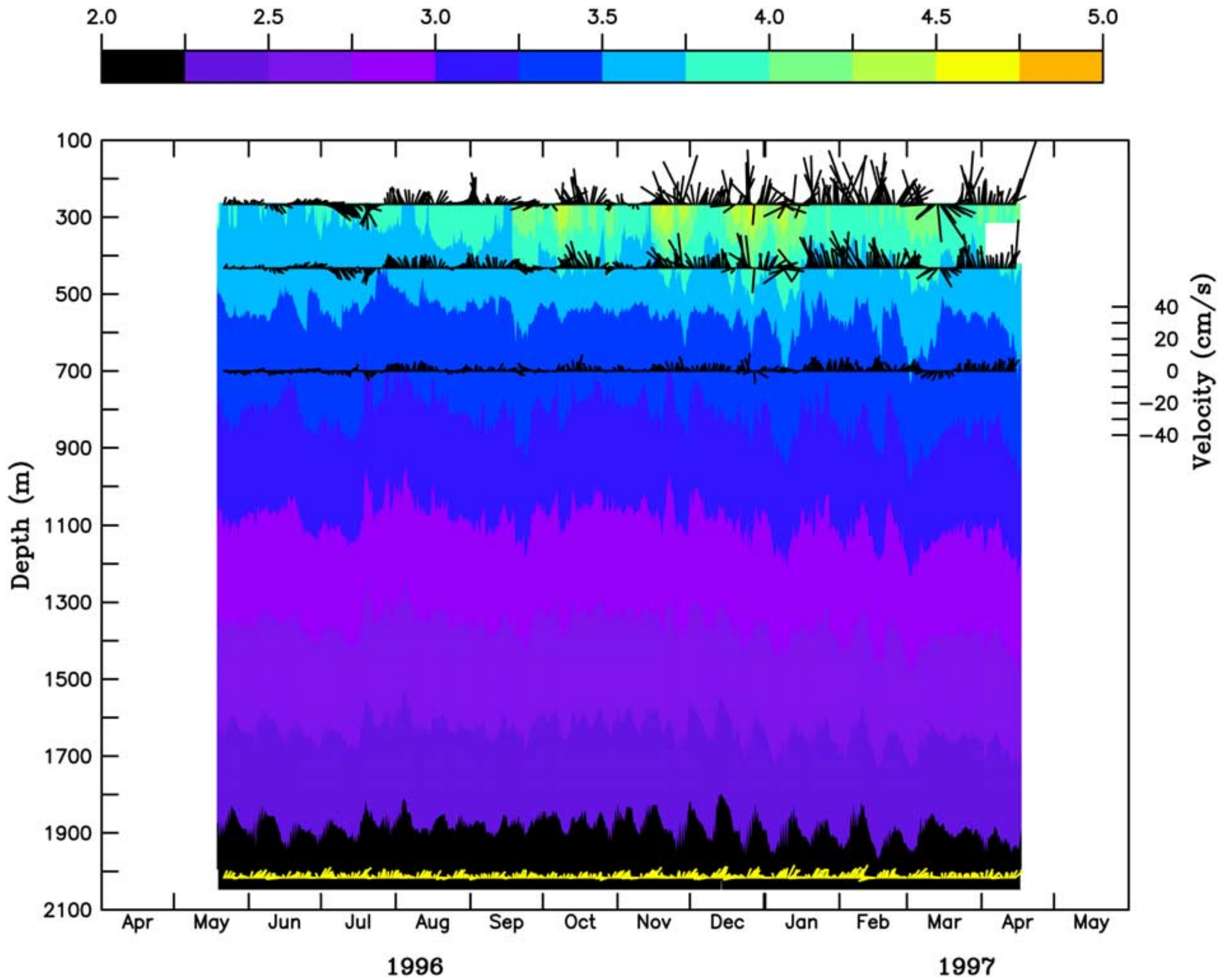

Figure 7. Temperature (in °C; color) and daily current vectors (rotated 60°, the net direction) measured at the mooring deployed at Site 7. The currents have been low-pass filtered. The position of the current time series indicates the approximate depth of instrument. Gaps in the records are due to failure of equipment.

the eddies is not as common at Site 6, where most of the variability was at a fortnightly period.

[41] One purpose of the dense vertical array of thermistors was to examine the subsurface maximum in temperature that is often observed in the southeastern Bering Sea basin. A seasonal subsurface temperature minimum overlays a deeper temperature maximum. Variability in the properties of the temperature maximum layer is due primarily to the strength of the inflow through Amukta Pass [*Reed*, 1995]. Profiles of temperature taken in the basin often have a subsurface temperature maximum at depths between 150 m and 350 m. The springtime section of temperature (Figure 5a), shows a subsurface maximum (>4°C) everywhere except at the station next to the Aleutian Islands. In fall and winter (Figures 5b and 5c), the relative maximum was weaker, with only a small area remaining where temperatures were above 4°C.

[42] Even though an examination of the time series from the moorings is limited by the lack of data in the upper 150 m, some patterns are evident (Figure 6). In the upper water column, cold temperatures (<3°C in 2000 and< 3.25°C in 1998) penetrated to a depth of ~300 m in winter and early spring. This is a signature of the strong vertical mixing in the passes, since over much of the southeast basin, winter mixing penetrates to a maximum depth of ~200 m [*Johnson et al.*, 2004]. A subsurface temperature maximum often occurred between 200 and 400 m for periods ranging from a few days (e.g., late February 1998) to over a month (e.g., late January–February 2000). During summer and fall, the occurrence of such a subsurface maximum was less common since temperatures above 200 m were warmer than those deeper in the water column.

6.2. Salinity

[43] At Site 6, time series of salinity at ~250 m show illustrate the seasonal variability (Figure 8). During June–November, salinity varied by about 0.2 with maximum salinity occurring in August in 1996 and 2000, and earlier in June in 1998. The lowest salinities occurred during winter.

[44] In December–May, the temporal variability increased markedly with the appearance of a series of "waves" with amplitudes of 0.3 to 0.5 and at fortnightly period. These waves are clearly evident in the wavelet analysis of the three salinity time series with significant energy of fortnightly timescales beginning in December and persisting at least until March (Figure 8). A similar wavelet analysis (not shown) of the total transport through Amukta Pass showed

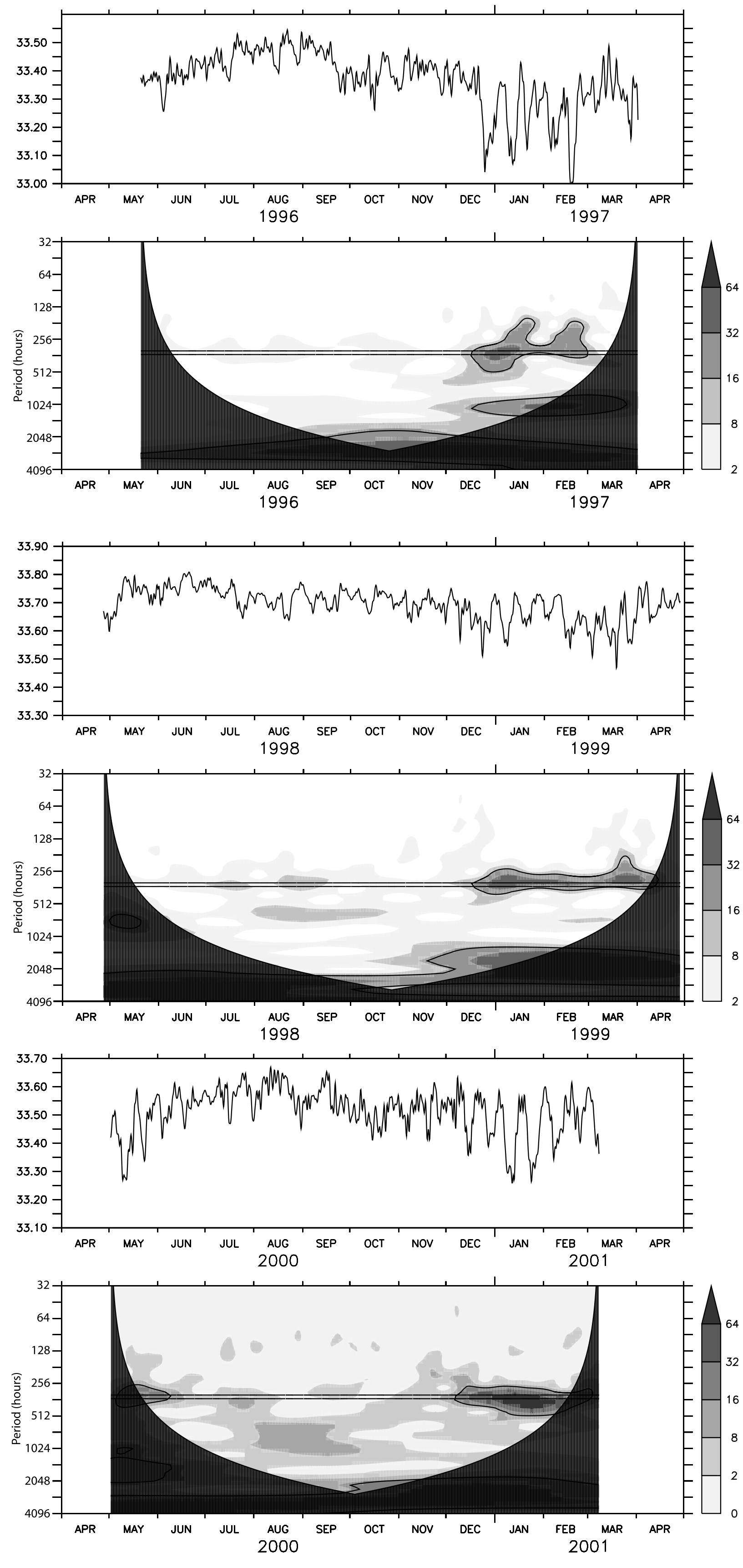
33.50
33.40
33.30
33.20
33.10
33.00
APR MAY JUN JUL AUG SEP OCT NOV DEC JAN FEB MAR APR
1996 1997
Period (hours)
32 64 128 256 512 1024 2048 4096
64 32 16 8 2
33.90
33.80
33.70
33.60
33.50
33.40
33.30
1998 1999
33.70
33.60
33.50
33.40
33.30
33.20
33.10
2000 2001
64 32 16 8 2 0

Figure 8

Table 3. Current Statistics From Moorings at Site 6

Location	Depth (m)	Duration of Record	Net Speed	Direction	$KE'/\overline{KE}$	Principal Axis (% Variance Explained)
		1996				
53°24.3′N, 168°50.5′W	293	19 May 1996 to 16 Apr 1997	9.9	20°	1.1	32° (78)
	593	2 May 1996 to 16 Apr 1997	4.0	16°	3.9	42° (80)
	943	21 May 1996 to 3 Jan 1997	3.1	15°	2.1	30° (88)
		1997				
53°24.3′N, 168°50.6′W	140	1 May 1997 to 23 Apr 1998	20.6	39°	0.4	39° (73)
	295	1 May 1997 to 23 Apr 1998	10.6	33°	1.3	40° (77)
	965	1 May 1997 to 23 Apr 1998	4.2	28°	0.9	27° (76)
		1998				
53°24.4′N, 168°50.9′W	240	24 Apr 1998 to 28 Nov 1998	12.7	39°	0.3	34° (77)
	385	24 Apr 1998 to 28 Apr 1999	6.5	35°	2.7	34° (81)
	1006	24 Apr 1998 to 28 Apr 1999	2.9	38°	0.5	40° (60)
		1999				
53°24.4′N, 168°51.1′W	278	29 Apr 1999 to 27 Apr 2000	10.3	34°	1.1	31° (78)
	966	29 Apr 1999 to 28 Apr 2000	2.9	12°	1.1	5° (72)
		2000				
53°24.4′N, 168°51.2′W	170	29 Apr 2000 to 20 Jun 2000	26.6	37°	0.3	5° (71)
	320	29 Apr 2000 to 11 Mar 2001	12.6	36°	1.3	25° (71)
	620	29 Apr 2000 to 11 Mar 2001	3.7	33°	6.6	43° (80)
	970	29 Apr 2000 to 11 Mar 2001	8.2	19°	0.6	27° (71)

fortnightly energy that persisted throughout the year not just from late fall into spring. At Site 6, the fortnightly signal was strongest at ~250 m, although it was also evident at 600 m. Similar temporal variability is evident in the currents measured at Site 6 as will be discussed below. Differences in salinity among years are difficult to quantify since the depth of the instruments varied slightly from year to year.

6.3. Currents

[45] Net flow in the ANSC and the axis of maximum variance were toward the northeast, paralleling the bathymetry (Table 3 and Figure 6). The average velocity decreased with depth from ~22 cm s^{-1} at ~150 m; ~11 cm s^{-1} at ~300 m; ~4 cm s^{-1} at ~600 m and ~4 cm s^{-1} near the bottom at ~950 m. At Site 6, the eddy kinetic energy/mean kinetic energy ratio was often less than 1, with the two largest values (3.9 and 6.6) at ~600 m. These eddy kinetic/mean kinetic energy ratios were similar to those measured in the Alaskan Stream [*Reed and Stabeno*, 1997; *Stabeno and Reed*, 1994]. There was considerable variability in current speed over the years, but the most surprising were the markedly higher bottom speeds during the fifth deployment (2000–2001). These higher speeds were similar to speeds observed at the same site in 2004 (not shown), and are likely a result of proximity to bathymetric features. The bottom is characterized by sharp gradients in bathymetry; if the mooring was deployed closer to one of these "cliffs," it would register higher flows near the bottom.

[46] Currents at the northern site (Site 7) were weaker and the direction was more northward than at Site 6 (Figures 6 and 7 and Table 4). The direction measured at the upper instruments was more variable than at Site 6. There also appears to be a significant annual signal in the velocity during 1996–1997 with higher flow during the winter. However, the flow at ~2000 m did not appear to vary annually. One of the interesting features is the relatively strong flow (~2.5 cm s^{-1}), modulated by fortnightly tides, near the bottom.

[47] The time series at the southern site (Site 6) reveal an annual signal in the velocity. From May through September, the flow was typically northeastward with few reversals. Starting in late fall, the currents became more energetic with an increase in the number of flow reversals. A marked semiannual cycle is evident in the along-shelf, monthly mean velocities at ~300 m, with a relative minimum in March/April and again in September/October (Figure 9). In contrast, the variance has a minimum during June, July, and August and a maximum in December perhaps because of increased variance in the winds (storminess) during winter. These are reflected in the eddy kinetic/mean kinetic energy ratios, which were small (<1.0) during summer and larger during spring and fall. The minimum in eddy kinetic/mean kinetic energy ratios during summer was a result of low variance and moderate mean velocity; the large (>4) eddy kinetic/mean kinetic energy ratios in March/April and September/October reflect the weak mean flow during those periods.

[48] The significant fortnightly signal in salinity occurred during fall and winter, coinciding with the period of increased reversals in current velocities. Similar fortnightly variability also occurred in temperature. An examination of a monthlong period in 2001 (Figure 10) shows the fortnightly variability

Figure 8. Salinity at ~250 m measured at Site 6 during three deployments (1996–1997, 1998–1999, and 2000–2001). The local wavelet power spectrum for each salinity time series is shown below the time series. The black contour encloses the region that is significant at the 95% confidence level for a red noise process. The black region indicates the "cone of influence" where edge effects become important. The horizontal black lines indicate lunisolar (327.86 h) and lunisolar synodic (354.37 h) fortnightly periods.

Table 4. Low-Pass Filtered Current Statistics From Mooring at Site 7 in 1996[a]

Location	Depth (m)	Net Speed	Direction	KE′/$\overline{\mathrm{KE}}$	Principal Axis (% Variance Explained)
53°36′N, 169°06′W	280	6.3	75°	3.4	48° (70)
	430	4.8	63°	2.8	39° (70)
	730	2.0	71°	3.9	45° (60)
	2030	2.5	65°	1.5	299° (93)

[a]Deployed 19 May 1996 to 17 April 1997.

in temperature, salinity and currents (low-pass filtered). During periods of stronger northeastward flow, the water column became less stratified while during periods of southwestward flow, the water column became more stratified. The mechanisms are not clear, but may be in response to the flow through and the mixing in Amukta and/or Amchitka Pass. Although transport in Amukta Pass has a strong fortnightly component, the pass is only ~400 m deep. The signal in the current meter records clearly extends to depth of ~1000 m. A fortnightly signal occurs in many of the deeper (>140 m)

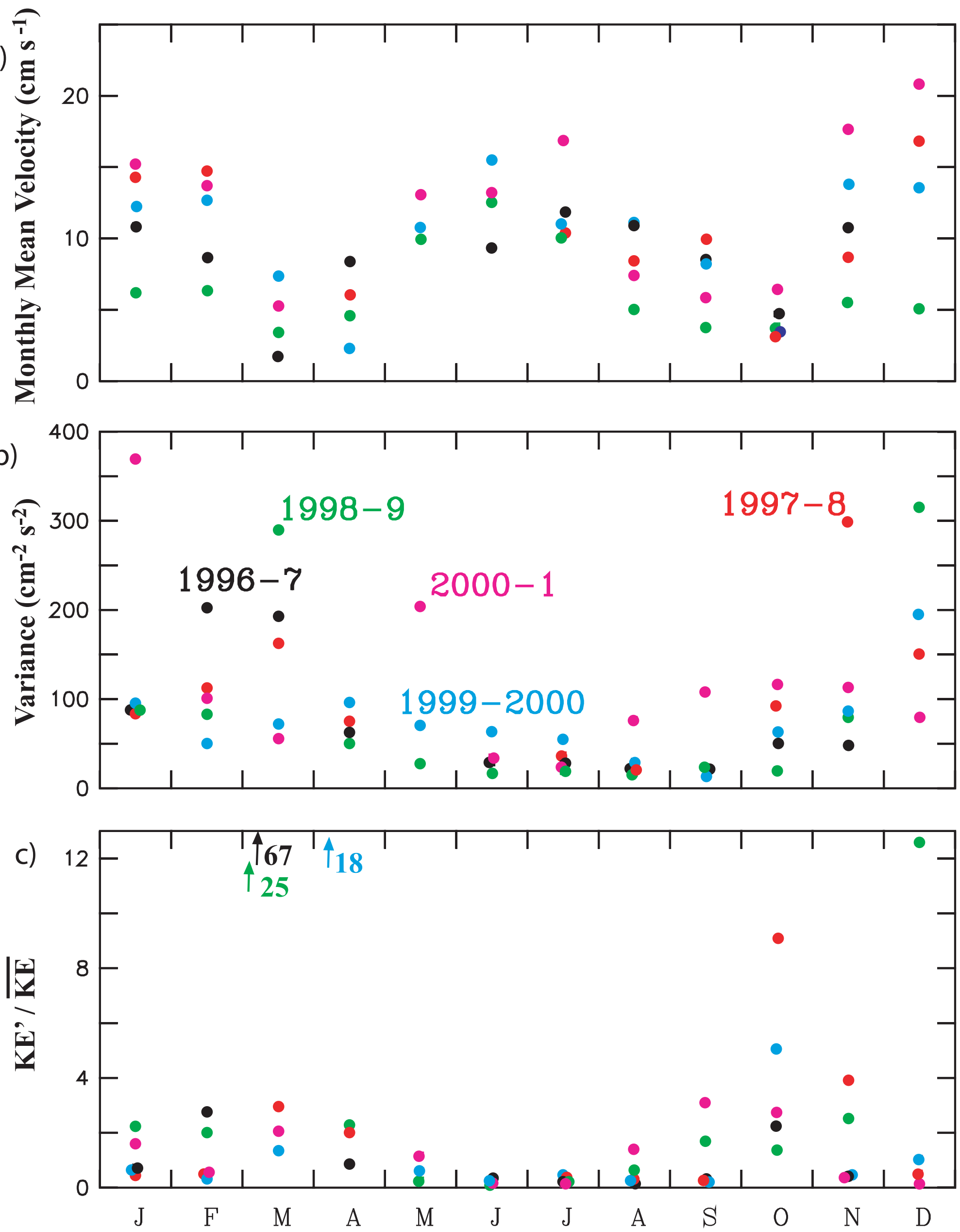

Figure 9. Data from moorings deployed at Site 6 at ~300 m. (a) Monthly mean along-shelf (rotated 30°) component of velocity. (b) Monthly variance of along-shelf velocity. (c) Eddy kinetic/mean kinetic energy ratio using data from Figures 9a and 9b. Years are represented by different colors as indicated in Figure 9b.

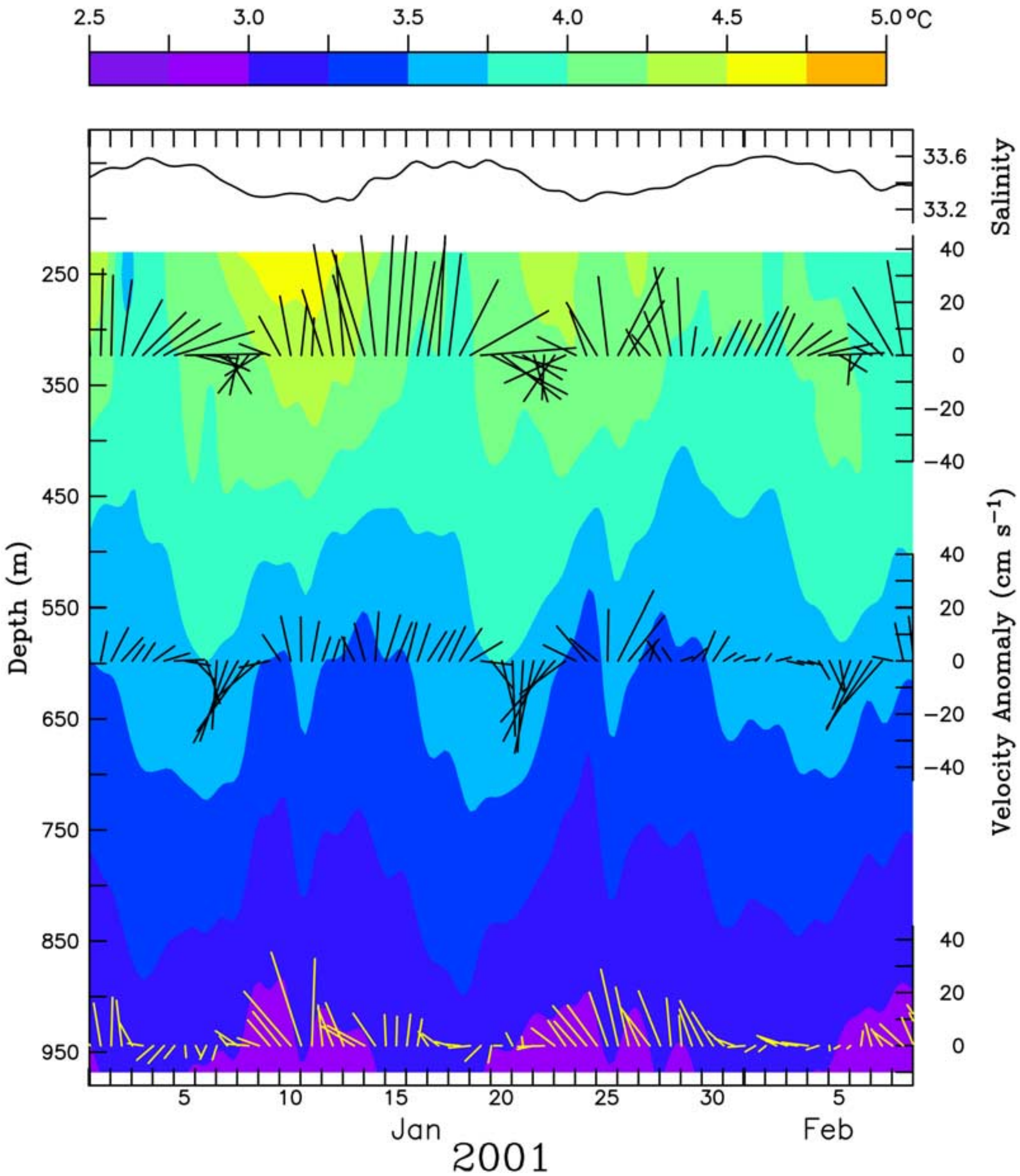

Figure 10. Temperature (in °C; color), salinity at ~250 m (black line), and 6 hourly current measured at the mooring deployed at Site 6. The currents were low-pass filtered and rotated 30°, so up is the along bathymetry (northeastward) flow. The position of the current time series indicates the depth of instrument.

Aleutian Passes including Near Strait. It would not be surprising if a fortnightly signal also modified flow through Amchitka Pass, the only eastern pass deeper than 1000 m.

7. Discussion and Conclusions

[49] While the geostrophic transport of the ANSC and BSC are highly correlated, other characteristics differ markedly between the two currents. The BSC is a typical eastern boundary current—broad, filled with eddies and meanders. In contrast, the ANSC looks like a western boundary current with its narrow, high-speed, strongly rectified flow. Both, however, are on the eastern boundary of the Bering Sea gyre. The mechanisms that result in the ANSC being a narrow, high-speed current with low-eddy kinetic energy (when compared to mean kinetic energy) are not known, but one possibility may be related to the fact that the Aleutian Arc is both narrow (often < 50 km) and porous. The Alaskan Stream is the western boundary current of the eastern subarctic gyre and the sea surface slopes upward toward the south side of the Aleutian Arc. The sea level height resulting from the stable Alaskan Stream could be transmitted through Aleutian Passes resulting in a stable sea level slope associated with the ANSC. The transmission of information (e.g., sea surface height) and/or the transport of water through the passes may act to stabilize the ANSC.

[50] On the hydrographic lines, baroclinic transport ranged from an eastward flow of almost 4×10^6 m^3 s^{-1} to $\sim 9 \times 10^6$ m^3 s^{-1} westward. The mean transport was $\sim 3 \times 10^6$ m^3 s^{-1}. The current meters nearest the bottom at the two mooring sites measured an average northeastward velocity of ~ 3 cm s^{-1}. Even relatively weak deep velocities can result in a large increase in the total transport. If 3 cm s^{-1} is taken to be

a depth-independent component of the ANSC spread over a width of 70 km and to an average depth of 1500 m, then the total barotropic component of transport would be $\sim 3 \times 10^6$ m^3 s^{-1}, a significant increase to the geostrophic ANSC transport (increasing the average from $\sim 3 \times 10^6$ m^3 s^{-1} to $\sim 6 \times 10^6$ m^3 s^{-1}). *Johnson et al.* [2004] calculated a similar barotropic transport in the BSC from Argo drifters, although they made no measurements for the ANSC because the Argo drifters could not resolve this narrow current. Even assuming the source waters for the ANSC are primarily the Aleutian Passes east of Amchitka Pass, these transports are not unreasonable. Transport was measured in several of the Aleutian Passes east of Amchitka Pass using moored current meters. Using these measurements, total transport through the passes to the east of Amchitka Pass was estimated to be 5–6 $\times 10^6$ m^3 s^{-1} [*Stabeno et al.*, 2005]. Amchitka Pass may also contribute significantly to the transport in the ANSC. In addition, some transport likely originates west of Amchitka Pass.

[51] The presence of a strong annual wind forcing cycle [*Bond et al.*, 1994] has been suggested to result in a well defined annual signal in the magnitude of the cyclonic transport in the Bering Sea basin [*Overland et al.*, 1994]. There does not appear to be a strong annual signal in the baroclinic transport presented in this paper. An examination of Table 1 reveals that the maximum transport (8.9×10^6 m^3 s^{-1}) and the largest counter (westward) transport (3.7×10^6 m^3 s^{-1}) in the ANSC were both in spring. The year-to-year variability in transport is so large that it would be difficult to detect an annual signal without a large number of observations spread throughout the year.

[52] Variability in velocities at Site 6 could indicate variability in ANSC transport and/or position. The semiannual signal in the monthly mean velocities (Figure 9) may be related to a semiannual signal in zonal wind stress. Westward winds in winter tend to position the Alaskan Stream closer to the Aleutian Islands, increasing transport through Amukta Pass [*Stabeno et al.*, 2005]. Eastward winds in summer have the opposite effect. This wind-driven variability in Amukta Pass transport likely results in variability in ANSC transport that may be reflected in currents at Site 6. Alternatively, changes in zonal wind stress could also change the position of the ANSC. This could also change the measured velocity at Site 6 (without changing the transport of the ANSC). Numerical models would be the best way to examine these mechanisms.

[53] Advection through and mixing in the Aleutian Passes is a dominant source of variability for the ANSC. The fortnightly variability that occurs in the Aleutian Passes is the most likely source of the fortnightly variability evident in the currents and salinities at Site 6. The deep mixing in the passes results in an annual temperature signal at >500 m, which is below the influence of local atmospheric mixing. Thus, the depth and the temperature of the subsurface temperature maximum in the Bering Sea are related to the variability in the strength and depth of mixing in the passes. Heat and salt are provided by the northward transport of Alaskan Stream water into the Bering Sea. The ANSC integrates the flux of Alaskan Stream water that enters the Bering Sea through various the Aleutian Passes and advects it northeastward; the BSC then transports the water northwestward providing heat and salt to the eastern Bering Sea shelf.

[54] **Acknowledgments.** We wish to thank W. Parker, W. Floering, C. Dewitt, and the crew and officers of the NOAA ship *Miller Freeman* for successful deployment of the moorings and the collection of the hydrography data. Altimetry data were provided by CLS Space Oceanography Division. Wavelet software was provided by C. Torrence and G. Compo and is available at URL http://atoc.colorado.edu/research/wavelets/. This is PMEL contribution 2459 and contribution FOCI-S559 to NOAA's Fisheries-Oceanography Coordinated Investigations.

References

Bond, N. A., J. E. Overland, and P. Turet (1994), Spatial and temporal characteristics of the wind forcing of the Bering Sea, *J. Clim.*, *7*, 1139–1143, doi:10.1175/1520-0442(1994)007<1139:SATCOT>2.0.CO;2.

Chen, S., and E. Firing (2006), Currents in the Aleutian Basin and subarctic North Pacific near the dateline in summer 1993, *J. Geophys. Res.*, *111*, C03001, doi:10.1029/2005JC003064.

Cherniawsky, J. Y., M. G. G. Foreman, W. R. Crawford, and R. F. Henry (2001), Ocean tides from TOPEX/Poseidon sea level data, *J. Atmos. Oceanic Technol.*, *18*, 649–664, doi:10.1175/1520-0426(2001)018<0649:OTFTPS>2.0.CO;2.

Cokelet, E. D., and P. J. Stabeno (1997), Mooring observations of the thermal structure, salinity, and currents in the SE Bering Sea basin, *J. Geophys. Res.*, *102*, 22,947–22,964, doi:10.1029/97JC00881.

Cummins, P. F., J. Y. Cherniawsky, and M. G. G. Foreman (2001), North Pacific internal tides from the Aleutian Ridge: Altimeter observations and modeling, *J. Mar. Res.*, *59*, 167–191, doi:10.1357/002224001762882628.

Ducet, N., P. Y. Le Traon, and G. Reverdin (2000), Global high-resolution mapping of ocean circulation from TOPEX/Poseidon and ERS-1 and -2, *J. Geophys. Res.*, *105*, 19,477–19,498, doi:10.1029/2000JC900063.

Favorite, F. (1974), Flow into the Bering Sea through Aleutian island passes, in *Oceanography of the Bering Sea With Emphasis on Renewable Resources*, edited by D. W. Hood and E. J. Kelley, pp. 3–37, Inst. of Mar. Sci., Univ. of Alaska, Fairbanks, Alaska.

Favorite, F., A. J. Dodimead, and K. Nasu (1976), Oceanography of the subarctic Pacific region, 1960–71, *Int. North Pac. Fish. Comm. Bull*, *33*, 187.

Johnson, G. C., P. J. Stabeno, and S. C. Riser (2004), The Bering Slope Current system revisited, *J. Phys. Oceanogr.*, *34*, 384–398, doi:10.1175/1520-0485(2004)034<0384:TBSCSR>2.0.CO;2.

Kinder, T. H., L. K. Coachman, and J. A. Galt (1975), The Bering Slope Current System, *J. Phys. Oceanogr.*, *5*, 231–244, doi:10.1175/1520-0485(1975)005<0231:TBSCS>2.0.CO;2.

Ladd, C., G. L. Hunt Jr., C. W. Mordy, S. A. Salo, and P. J. Stabeno (2005), Marine environment of the eastern and central Aleutian Islands, *Fish. Oceanogr.*, *14*, 22–38, doi:10.1111/j.1365-2419.2005.00373.x.

Le Traon, P. Y., and G. Dibarboure (1999), Mesoscale mapping capabilities of multi-satellite altimeter missions, *J. Atmos. Oceanic Technol.*, *16*, 1208–1223, doi:10.1175/1520-0426(1999)016<1208:MMCOMS>2.0.CO;2.

Le Traon, P. Y., and G. Dibarboure (2004), An illustration of the contribution of the TOPEX/Poseidon-Jason-1 tandem mission to mesoscale variability studies, *Mar. Geod.*, *27*, 3–13, doi:10.1080/01490410490489313.

Le Traon, P. Y., F. Nadal, and N. Ducet (1998), An improved mapping method of multi-satellite altimeter data, *J. Atmos. Oceanic Technol.*, *15*, 522–534, doi:10.1175/1520-0426(1998)015<0522:AIMMOM>2.0.CO;2.

Mordy, C. W., P. J. Stabeno, C. Ladd, S. Zeeman, D. P. Wisegarver, and G. L. Hunt Jr. (2005), Nutrients and primary production along the eastern Aleutian Island Archipelago, *Fish. Oceanogr.*, *14*, 55–76, doi:10.1111/j.1365-2419.2005.00364.x.

Overland, J. E., M. C. Spillane, H. E. Hurlburt, and A. J. Wallcraft (1994), A numerical study of the circulation of the Bering Sea Basin and exchange with the North Pacific Ocean, *J. Phys. Oceanogr.*, *24*, 736–758, doi:10.1175/1520-0485(1994)024<0736:ANSOTC>2.0.CO;2.

Panteleev, G. G., P. Stabeno, V. A. Luchin, D. A. Nechaev, and M. Ikeda (2006), Summer transport estimates of the Kamchatka Current derived as a variational inverse of hydrophysical and surface drifter data, *Geophys. Res. Lett.*, *33*, L09609, doi:10.1029/2005GL024974.

Reed, R. K. (1990), A year-long observation of water exchange between the North Pacific and the Bering Sea, *Limnol. Oceanogr.*, *35*, 1604–1609.

Reed, R. K. (1995), On the variable subsurface environment of fish stocks in the Bering Sea, *Fish. Oceanogr.*, *4*, 317–323, doi:10.1111/j.1365-2419.1995.tb00076.x.

Reed, R. K., and P. J. Stabeno (1994), Flow along and across the Aleutian Ridge, *J. Mar. Res.*, *52*, 639–648, doi:10.1357/0022240943076957.

Reed, R. K., and P. J. Stabeno (1997), Long-term measurements of flow near the Aleutian Islands, *J. Mar. Res.*, *55*, 565–575, doi:10.1357/0022240973224328.

Reed, R. K., and P. J. Stabeno (1999a), The Aleutian North Slope Current, in *Dynamics of the Bering Sea*, edited by T. R. Loughlin and K. Ohtani, pp. 177–191, Univ. of Alaska Sea Grant, Fairbanks, Alaska.

Reed, R. K., and P. J. Stabeno (1999b), A recent full-depth survey of the Alaskan Stream, *J. Oceanogr.*, *55*, 79–85, doi:10.1023/A:1007813206897.

Sayles, M. A., K. Aagaard, and L. K. Coachman (1979), *Oceanographic Atlas of the Bering Sea Basin*, 158 pp., Univ. of Washington Press, Seattle, Wash.

Stabeno, P. J., and R. K. Reed (1994), Circulation in the Bering Sea basin observed by satellite-tracked drifters: 1986–1993, *J. Phys. Oceanogr.*, *24*, 848–854, doi:10.1175/1520-0485(1994)024<0848:CITBSB>2.0.CO;2.

Stabeno, P. J., and P. Van Meurs (1999), Evidence of episodic on-shelf flow in the southeastern Bering Sea, *J. Geophys. Res.*, *104*, 29,715–29,720, doi:10.1029/1999JC900242.

Stabeno, P. J., J. D. Schumacher, and K. Ohtani (1999), The physical oceanography of the Bering Sea, in *Dynamics of the Bering Sea*, edited by T. R. Loughlin and K. Ohtani, pp. 1–28, Univ. of Alaska Sea Grant, Fairbanks, Alaska.

Stabeno, P. J., N. A. Bond, N. B. Kachel, S. A. Salo, and J. D. Schumacher (2001), On the temporal variability of the physical environment over the south-eastern Bering Sea, *Fish. Oceanogr.*, *10*, 81–98, doi:10.1046/j.1365-2419.2001.00157.x.

Stabeno, P. J., R. K. Reed, and J. M. Napp (2002), Transport through Unimak Pass, Alaska, *Deep Sea Res., Part II*, *49*, 5919–5930, doi:10.1016/S0967-0645(02)00326-0.

Stabeno, P. J., D. G. Kachel, N. B. Kachel, and M. E. Sullivan (2005), Observations from moorings in the Aleutian Passes: Temperature, salinity and transport, *Fish. Oceanogr.*, *14*, 39–54, doi:10.1111/j.1365-2419.2005.00362.x.

Torrence, C., and G. P. Compo (1998), A practical guide to wavelet analysis, *Bull. Am. Meteorol. Soc.*, *79*, 61–78, doi:10.1175/1520-0477(1998)079<0061:APGTWA>2.0.CO;2.

Wirts, A. E., and G. C. Johnson (2005), Recent interannual upper ocean variability in the deep southeastern Bering Sea, *J. Mar. Res.*, *63*, 381–405, doi:10.1357/0022240053693725.

C. Ladd, R. K. Reed, and P. J. Stabeno, Pacific Marine Environmental Laboratory, NOAA, 7600 Sand Point Way, NE, Seattle, WA 98115-6349, USA. (stabeno@noaa.gov)